



Fracture in elongational flow of two low-density polyethylene melts

Leslie Poh^{1,2} · Qi Wu^{1,2} · Zhengbin Pan^{1,2} · Manfred H. Wagner³ · Esmail Narimissa^{1,2}

Received: 11 January 2023 / Revised: 1 March 2023 / Accepted: 11 March 2023 / Published online: 6 June 2023
© The Author(s) 2023

Abstract

Samples of two commercial low-density polyethylene melts were investigated with respect to their fracture behavior in controlled uniaxial extensional flow at constant strain rate in a filament stretching rheometer. In order to assess the possible influence of grain boundaries on fracture, the samples were prepared by three different types of pre-treatment: by compression molding of (1) virgin pellets used as received, (2) pellets homogenized in a twin-screw extruder, and (3) pellets that were milled into powder by cryogenic grinding under liquid nitrogen. The elongational stress growth data were analyzed by the Extended Hierarchical Multi-mode Molecular Stress Function (EHMMSF) model developed by Wagner et al. (Rheol. Acta 61, 281–298 (2022)) for long-chain branched (LCB) polymer melts. The EHMMSF model quantifies the elongational stress growth including the maximum in the elongational viscosity of LDPE melts based solely on the linear-viscoelastic relaxation spectrum and two nonlinear material parameters, the dilution modulus G_D and a characteristic stretch parameter λ_m . Within experimental accuracy, model predictions are in excellent agreement with the elongational stress growth data of the two LDPE melts, independent of the preparation method used. At sufficiently high strain rates, the fracture of the polymer filaments was observed and is in general accordance with the entropic fracture criterion implemented in the EHMMSF model. High-speed videography reveals that fracture is preceded by parabolic crack opening, which is characteristic for elastic fracture and which has been observed earlier in filament stretching of monodisperse polystyrene solutions. Here, for the first time, we demonstrate the appearance of a parabolic crack opening in the fracture process of polydisperse long-chain branched polyethylene melts.

Keywords Fracture of polymer melts · Entropic fracture criterion · Parabolic crack opening · Filament stretching rheometry · Elongational viscosity · Viscosity overshoot · Branch point withdrawal · EHMMSF model

Introduction

Low-density polyethylene (LDPE) consists of short- and long-chain branched macromolecules with widely different structures including hyper-branching with branch-on-branch topologies and LDPE is therefore one of the most complex

entangled polymer system. It is therefore highly challenging to predict the rheological behavior of LDPEs, especially the nonlinear viscoelastic behavior including the fracture in extensional flows. While linear polymer melts show a monotonously increasing elongational stress growth coefficient with increasing time or deformation reaching finally a steady-state elongational viscosity, long-chain branched (LCB) polymers display an overshoot of the transient elongational viscosity at high strains and strain rates if the samples do not fracture earlier. Previous reports concerning the existence of elongational viscosity overshoot of LCB melts were reviewed recently by Wagner et al. (2022), together with earlier attempts to predict the viscosity overshoot of LDPE, such as the pom-pom model of McLeish and Larson (1998), which is based on the idea of “branch point withdrawal,” i.e., the branch points and side arms are withdrawn into the backbone tube at sufficiently large deformation. Wagner et al. (2022) also considered the entropic fracture

✉ Leslie Poh
leslie.pohpingyi@gmail.com

✉ Manfred H. Wagner
manfred.wagner@tu-berlin.de

¹ Dept. of Chemical Engineering, Technion–Israel Institute of Technology (IIT), Technion City, 32 000 Haifa, Israel

² Dept. of Chemical Engineering, Guangdong Technion–Israel Institute of Technology (GTIIT), Shantou 515063, China

³ Polymer Engineering/Polymer Physics, Berlin Institute of Technology (TU Berlin), Ernst-Reuter-Platz 1, 10587 Berlin, Germany

criterion. According to this criterion, a polymer will fail by fracture when the stretch energy of entanglement segments reaches the bond-dissociation energy of a single carbon-carbon bond. Due to thermal fluctuations, the energy will be rapidly concentrated on one bond, and the bond then ruptures. This leads to crack initiation and within a very short time, to brittle fracture of the sample.

The significance of the nonlinear rheological modeling of polydisperse polymeric systems for quantitative flow and fracture simulations in polymer processing has prompted Narimissa et al. (2015, 2016), and Narimissa and Wagner (2016a, b, c) to develop the Hierarchical Multi-mode Molecular Stress Function (HMMSF) model capable of predicting the rheological behaviors of linear and long-chain branched polymers for various categories of flow, i.e., elongational, multiaxial extensional, and shear deformations, based on the linear-viscoelastic (LVE) characterization of the melt and only two free nonlinear parameters (i.e., 1 in extensional flows and 2 in shear flow). The basic idea in the development of the model has been to recognize that the rheological effects of the complex (and in the case of long-chain branched polymers often unknown) molecular structures are already contained in the linear-viscoelastic spectrum of relaxation times of the polymer and that only a limited number of well-defined constitutive assumptions concerning the nonlinear rheology is needed, thereby reducing the number of adjustable free nonlinear material parameters to a minimum. The HMMSF model is based on the linear-viscoelastic relaxation modulus, and the concepts of hierarchical relaxation, dynamic dilution, and interchain tube pressure. It was shown to predict the elongational and multiaxial extensional viscosities as well as the shear viscosity of several polydisperse linear polymer melts based exclusively on their linear-viscoelastic characterization by use of a single nonlinear material parameter, the so-called dilution modulus G_D , for extensional flows, and in addition, a constraint release parameter for shear flow. For long-chain branched polymer melts, the HMMSF describes accurately the elongational stress growth coefficient up to the maximum of the elongational viscosity, but fails to predict the existence of a maximum and the following steady-state viscosity at higher strain rates. This maximum in the elongational stress growth coefficient can be accounted for by the Extended Hierarchical Multi-mode Molecular Stress Function (EHMMSF) model (Wagner et al. 2022), which introduces a stretch parameter characterizing the specific strain at the maximum of the tensile stress and therefore the beginning of branch point withdrawal. The EHMMSF model also quantifies the stretch energy of entanglement strands, which is the input for the entropic fracture criterion.

The objectives of this contribution are to investigate the fracture behavior of two LDPE melts in elongational flow. In order to assess the possible influence of grain boundaries

on fracture, we used three different types of sample preparation: Samples were produced from (1) virgin pellets used as received, (2) pellets that were homogenized in a twin-screw extruder, and (3) pellets that were milled into powder form using cryogenic grinding under liquid nitrogen. Assessing the effect of different pre-treatments on the rheology of LCB polymers and their fracture behavior is also of considerable interest for compounding and recycling of polymers. The paper is organized as follows: First, we give an account of the materials and experimental methods, which is followed by a short summary of the HMMSF model and the fracture criterion. Then, the molecular and the linear-viscoelastic characteristics of the LDPE samples are reported, and the experimental data of the transient elongational viscosity are compared to the HMMSF and the EHMMSF models as well as the entropic fracture criterion. Finally, optical observations by high-speed videography of brittle fracture in elongational flow are reported, followed by discussion and conclusions.

Materials and methods

Materials

LDPE Purell 1840H polymer in pellet form was purchased from LyondellBasell and LDPE 3020D polymer pellets were provided by Technische Universität Berlin. We employed three different pre-treatment methods to produce test samples from the two LDPEs investigated: Samples which were compression molded from virgin pellets as received are denoted by “V,” samples which were produced from pellets that were homogenized in a twin-screw extruder at 170 °C are denoted by “E,” and samples produced from pellets that are ground into powder form using cryogenic grinding with liquid nitrogen are denoted by “P.” All the LDPE samples were dried in a vacuum oven at 50 °C for 24 h to remove moisture before compression molding.

Experimental methods

The molecular weights and molecular weight distributions of LDPE 1840H and LDPE 3020D samples were determined by gel permeation chromatography (GPC) using a PL-GPC-200 instrument equipped with a differential detector and two PLgel MIXED-LS 300 × 7.5 mm columns. The measurements were performed at 150 °C with 1,2,4-trichlorobenzene as the eluent at a flow rate of 1 mL/min with polystyrene as the calibration standard. The branching level $CH_3/1000C$ of LDPEs was calculated using 1H nuclear magnetic resonance (NMR) data. NMR was recorded on a 400 MHz Bruker AVANCE III instrument at 120 °C using

deuterated 1,2-dichlorobenzene as the solvent with sample concentration of 80 mg/mL.

The densities of the LDPE samples were measured using a gas pycnometer (Accupyc 1345, Micromeritics) with a helium gas pressure of 19.5 psig and chamber size of 10 cm³. Thermal properties of LDPE 1840H and LDPE 3020D samples were analyzed using differential scanning calorimetry (DSC25, TA Instruments). Samples of about 5 mg were heated to 200 °C to remove their thermal history and cooled to −90 °C, and a second heating cycle was conducted at a temperature range of −90 to 200 °C. The experiment used a heating rate of 10 °C/min and a cooling rate of 5 °C/min under a nitrogen atmosphere with a flow rate of 50 mL/min. Only the second heating cycle was considered to determine the crystallinity of the samples.

Linear-viscoelastic (LVE) properties of the low-density polyethylene melts were obtained from small amplitude oscillatory shear (SAOS). SAOS measurements for LDPE 1840H and LDPE 3020D samples were performed using 25-mm-parallel plate geometry on an ARES-G2 rheometer from TA Instruments. The LDPE 1840H and LDPE 3020D samples were compression molded at approximately 150 °C for 15 min into disk-shaped samples with 25 mm diameter for the SAOS measurements. The measurements for LDPE 1840H were carried out at 150, 170, and 190 °C with two sets of multi-wave oscillations at each temperature. The measurements for LDPE 3020D were carried out at 130, 150, 170, and 190 °C with two sets of multi-wave oscillations at each temperature. The fundamental and harmonic frequencies for the multi-wave oscillation are summarized in Table 1. All data for LDPE 1840H and LDPE 3020D were shifted to 150 and 130 °C, respectively, using the time-temperature-superposition procedure.

Elongational stress measurements for LDPE 1840H and LDPE 3020D were performed using a VADER 1000 (Rheo Filament ApS, Albertslund, DK) at 150 and 130 °C,

respectively. The LDPE 1840H and LDPE 3020D samples used for the extensional measurements were compression molded at 150 °C for 15 min into cylindrical test samples with a radius of $R_0 = 3.1$ mm and pre-stretched to a radius of 2.9 mm and a length of $L_0 = 2.2$ mm.

Videography of fracture experiments was performed using a high-speed camera (Photron FASTCAM Nova S12) with a 105 mm f/2.8 Micro-Nikkor lens and a high-power LED lamp (Veritas MiniConstellation 120 5000 K) coupled with a VADER 1000 at a stretch rate of 3.0 s^{−1} at 130 °C using 16,000 and 25,000 frames per second for LDPE 1840H and 3020D samples, respectively. Slower frame rates were used for 1840H to extend the capture time as a longer experimental time up to fracture was needed for 1840H as compared to 3020D. The extensional measurements carried out on VADER 1000 were performed using feedforward control parameters (Román Marin et al. 2013) that define the kinematic trajectory of the top plate motor in a close loop scheme with active feedback control.

The EHMSF model and the entropic fracture criterion

The Hierarchical Multi-Mode Molecular Stress Function (HMMSF) model was developed by Narimissa et al. (2015, 2016), and Narimissa and Wagner (2016a, b, c) for the prediction of uniaxial, multiaxial, and shear rheological behaviors of polydisperse long-chain branched (LCB) polymer melts as well as polydisperse linear melts. A summary of the development of the HMMSF model was presented by Narimissa and Wagner (2019a), a comparison between this model and other prominent tube-models for polydisperse linear and long-chain branched polymer melts was given by Narimissa and Wagner (2019b). At Hencky strains greater than $\epsilon \approx 4$ and higher strain rates, the elongational stress growth coefficient of long-chain branched (LCB) polymer melts such as low-density polyethylene (LDPE) shows an overshoot due to branch point withdrawal before reaching a steady-state elongational viscosity. This can be accounted for by the Extended Hierarchical Multi-mode Molecular Stress Function (EHMSF) model as explained in detail by Wagner et al. (2022), which introduces a stretch parameter characterizing the specific Hencky strain at the maximum of the tensile stress. The extra stress tensor of the EHMSF model is given by

$$\sigma(t) = \sum_i \int_{-\infty}^t \frac{\partial G_i(t-t')}{\partial t'} H_i(t,t') f_i^2(t,t') \mathbf{S}_{DE}^{IA}(t,t') dt' \quad (1)$$

Here, \mathbf{S}_{DE}^{IA} is the Doi and Edwards strain tensor assuming an independent alignment (IA) of tube segments (Doi

Table 1 Fundamental and harmonic frequencies for multi-wave oscillations used for LDPE 1840H and LDPE 3020D

First step			Second step	
Frequency (rad/s)	Amplitude (%)		Frequency (rad/s)	Amplitude (%)
ω_0	0.01	3	1	3
ω_1	0.03	2	3	2
ω_2	0.06	2	6	2
ω_3	0.1	1	10	1
ω_4	0.16	1	16	1
ω_5	0.32	1	32	1
ω_6	1	0.2	100	0.2
ω_7	2.56	0.1	256	0.1
Peak strain	-	6.65	-	6.65

Table 2 Molecular weight (M_w), polydispersity index (M_w/M_n), degree of branching, density, and crystallinity of LDPE 1840H and LDPE 3020D with different pre-treatments

Sample	M_w (g/mol)	M_w/M_n	CH ₃ /1000C	ρ (g/cm ³)	X_c (%)
LDPE 1840H-V	89,253	4.25	31	0.9201	47.92
LDPE 1840H-E	91,855	4.53	23	0.9207	48.88
LDPE 1840H-P	89,508	3.50	22	0.9256	50.99
LDPE 3020D-V	109,707	3.79	21	0.9212	49.66
LDPE 3020D-E	99,941	3.93	28	0.9234	50.92
LDPE 3020D-P	101,774	3.59	18	0.9272	51.36

and Edwards 1978), which is five times the second-order orientation tensor S ,

$$S_{DE}^{IA}(t, t') \equiv 5 \left\langle \frac{\mathbf{u}'\mathbf{u}'}{u'^2} \right\rangle = 5S(t, t') \quad (2)$$

u' presents the length of the deformed unit vector \mathbf{u}' , and the bracket denotes an average over an isotropic distribution of unit vectors at time t' , $\mathbf{u}(t')$, which can be expressed as a surface integral over the unit sphere,

$$\langle \dots \rangle_o = \frac{1}{4\pi} \iint [\dots] \sin \theta_o d\theta_o d\varphi_o \quad (3)$$

The relative deformation gradient tensor, $\mathbf{F}^{-1}(t, t')$, signifies the deformation of the unit vector \mathbf{u} at observation time t to \mathbf{u}' according to the affine deformation assumption,

$$\mathbf{u}'(t, t') = \mathbf{F}^{-1}(t, t') \cdot \mathbf{u}(t') \quad (4)$$

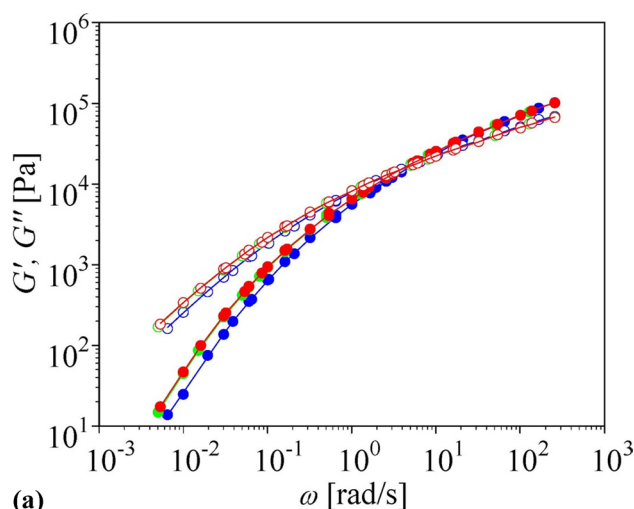
The molecular stress functions $f_i = f_i(t, t')$ are the inverse of the relative tube diameters a_i of each mode i ,

$$f_i(t, t') = a_{i0}/a_i(t, t') \quad (5)$$

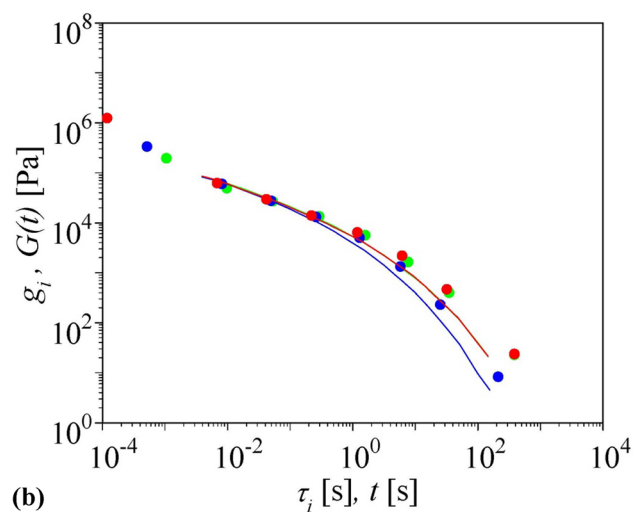
$f_i = f_i(t, t')$ is a function of both the observation time t and the time t' of the creation of tube segments by reptation. The relaxation modulus $G(t)$ of the melt is represented by discrete Maxwell modes with partial relaxation moduli g_i and relaxation times τ_i ,

$$G(t) = \sum_j^n G_j(t) = \sum_j^n g_j \exp(-t/\tau_j) \quad (6)$$

We use parsimonious relaxation spectra as determined by the IRIS software (Winter and Mours 2006; Poh et al. 2022a) by fitting SAOS data. It is important realizing that the hierarchical relaxation and dilution of the tube



(a)



(b)

Fig. 1 a Storage (G') and loss modulus (G'') of LDPE 1840H (V green, E red, P blue) at reference temperature $T = 150$ °C. b Partial relaxation moduli $g_i(\tau_i)$ (symbols) and relaxation modulus $G(t)$ (lines) as determined by the IRIS software (Winter and Mours 2006; Poh et al. 2022a)

are already embedded in the linear-viscoelastic relaxation spectrum and can therefore be extracted from the spectrum as shown in the following.

The evolution equation for the molecular stress function of each mode is expressed as,

$$\frac{\partial f_i}{\partial t} = f_i(\mathbf{K} : \mathbf{S}) - \frac{f_i - 1}{\alpha\tau_i} \left(1 - \frac{2}{3}w_i^2\right) - \frac{2f_i^2(f_i^3 - 1)}{3 \cdot 3\alpha\tau_i} w_i^2 \quad (7)$$

with the initial conditions $f_i(t=t', t') = 1$ (Narimissa and Wagner 2016b, 2019a). The first term on the right hand side represents an on average affine stretch rate with \mathbf{K} the velocity gradient tensor, the second term takes into account Rouse relaxation in the longitudinal direction of the tube, and the third term limits molecular stretch due

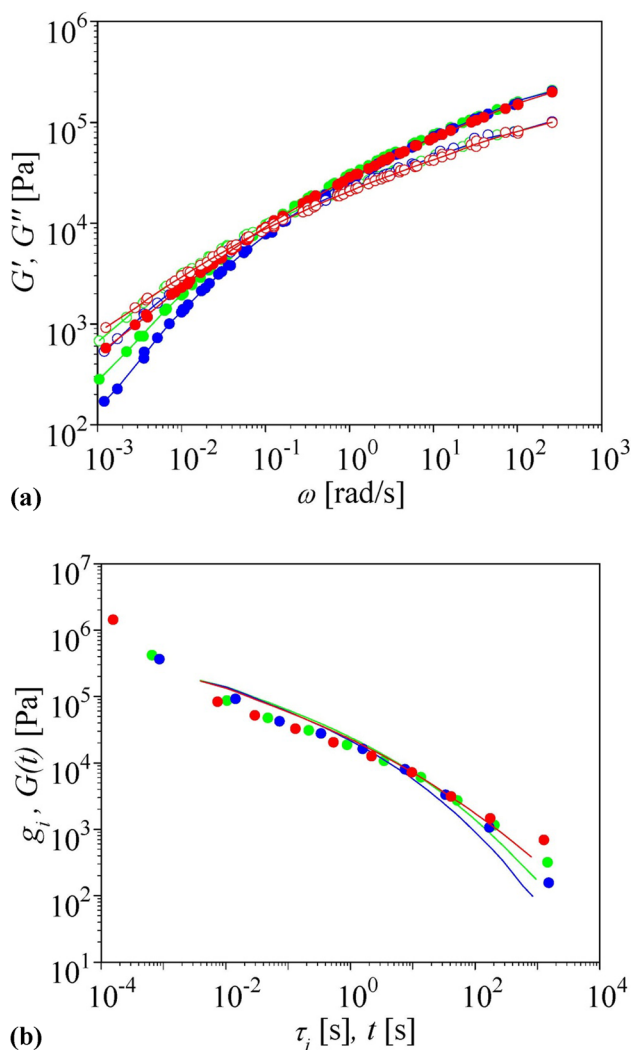


Fig. 2 **a** Storage (G') and loss modulus (G'') of LDPE 3020D (V green, E red, P blue) at reference temperature $T = 130$ °C. **b** Partial relaxation moduli $g_i(\tau_i)$ (symbols) and relaxation modulus $G(t)$ (lines) as determined by the IRIS software (Winter and Mours 2006; Poh et al. 2022a)

to the interchain tube pressure in the lateral direction of a tube segment (Wagner et al. 2005; Wagner and Rolón-Garrido 2009a, b). The effect of dynamic dilution is entering Eq. (7) via the square of the weight fractions, w_i^2 ,

Table 3 Zero-shear viscosity η_0 , dilution modulus G_D , and characteristic stretch parameter $\bar{\lambda}_m$ at reference temperature T

Sample	T (°C)	η_0 (kPa s)	G_D (kPa)	$\bar{\lambda}_m$ (-)
LDPE 1840H-V	150	36.2	10	90
LDPE 1840H-E	150	36.9	10	90
LDPE 1840H-P	150	27.2	10	90
LDPE 3020D-V	130	988	3	40
LDPE 3020D-E	130	1375	3	60
LDPE 3020D-P	130	631	3	40

and takes into account that the effect of dynamic dilution vanishes in fast flows as discussed in Wagner (2011). The weight fraction w_i of a dynamically diluted linear or LCB polymer segment with relaxation time $\tau_i > \tau_D$ is determined by considering the ratio of the relaxation modulus at time $t = \tau_i$ to the dilution modulus $G_D = G(t = \tau_D)$,

$$w_i^2 = \frac{G(t=\tau_i)}{G_D} = \frac{1}{G_D} \sum_{j=1}^n g_j \exp(-\tau_i/\tau_j) \text{ for } \tau_i > \tau_D \quad (8)$$

$$w_i^2 = 1 \text{ for } \tau_i \leq \tau_D$$

It is assumed that the value of w_i obtained at $t = \tau_i$ can be attributed to the chain segments with relaxation time τ_i . Segments with $\tau_i < \tau_D$ are considered to be permanently diluted, i.e., their weight fractions are fixed at $w_i = 1$. Dynamically diluted chain segments with $\tau_i > \tau_D$ have weight fractions $w_i < 1$, which lead to higher values of the molecular stress functions f_i according to Eq. (7). Thus, dynamic dilution leads to enhanced stretch and enhanced strain hardening in elongational flow. As shown by Narimissa et al. (2015), these assumptions allow modeling the rheology of broadly distributed polymers, largely independent of the number of discrete Maxwell modes used to represent the relaxation modulus $G(t)$.

The topological parameter α depends on the topology of the melt (Narimissa and Wagner 2019a), with

$$\alpha = 1 \text{ for LCB Melts}$$

$$\alpha = 1/3 \text{ for polydisperse linear melts} \quad (9)$$

The original HMMSF model is retained from Eq. (1) for

$$H_i(t, t') = 1 \quad (10)$$

At sufficiently large and fast deformations, branch point withdrawal will occur in LCB melts, i.e., branch points and side arms will be withdrawn into the backbone tube and the number of effective entanglements carrying stress will decrease. Restricting attention to increasing deformations, we model this effect by dimensionless functions H_i representing the percentage of entanglements with relaxation times τ_i surviving a given deformation,

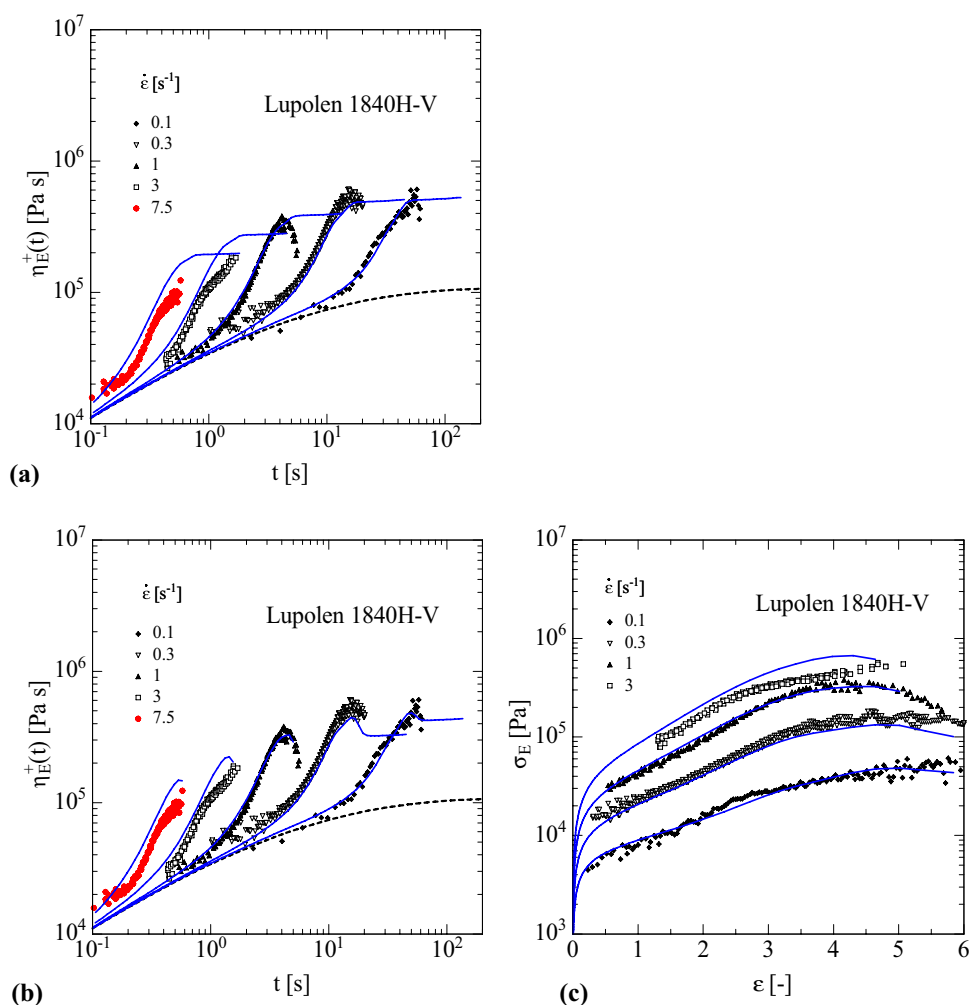
$$H_i(t, t') = \left[1 + \frac{w_i \tau_i \mathbf{K} : \mathbf{S}(t, t')}{1 + (\bar{\lambda}_m / \bar{\lambda}(t, t'))^4} \right]^{-1} \quad (11)$$

$\bar{\lambda}(t, t')$ is the average affine stretch of an entanglement segment between the times t and t' without the consideration of stretch relaxation (Wagner et al. 2022),

$$\bar{\lambda}(t, t') = \exp(\langle \ln u'(t, t') \rangle_0) \quad (12)$$

$\bar{\lambda}(t, t')$ can also be considered as a normalized strain energy function and is a frame invariant quantity. The parameter $\bar{\lambda}_m$

Fig. 3 Comparison of data (symbols) of elongational stress growth coefficient $\eta_E^+(t)$ for LDPE 1840H-V at 150 °C to HMMSF model (lines) with $G_D = 10$ kPa (a), and to EHMMSF model (lines) with $G_D = 10$ kPa and $\bar{\lambda}_m = 90$ (b). Data at $\dot{\epsilon} = 7.5s^{-1}$ were measured at 130 °C and are time-temperature shifted to 150 °C. c Comparison of data (symbols) of elongational stress growth $\sigma_E(\epsilon)$ to EHMMSF model (lines) with $G_D = 10$ kPa and $\bar{\lambda}_m = 90$



represents a measure of the characteristic stretch (or strain energy) defining the maximum of the elongational viscosity. As shown by Wagner et al. (2022), $\bar{\lambda}_m$ can be converted in good approximation into an equivalent characteristic Hencky strain $\epsilon_m = 1 + \ln(\bar{\lambda}_m)$. The larger the value of $\bar{\lambda}_m$, the larger is the Hencky strain at which the maximum in the tensile start-up stress $\sigma_E(\epsilon)$ or in the elongational stress growth coefficient $\eta_E^+(t)$ is reached. A large value of $\bar{\lambda}_m$ is associated with a polymer topology featuring a large number and/or rather long side chains with possibly branch-on-branch topology resulting in large deformations and thereby large tensile forces in the backbone chain required for branch point withdrawal.

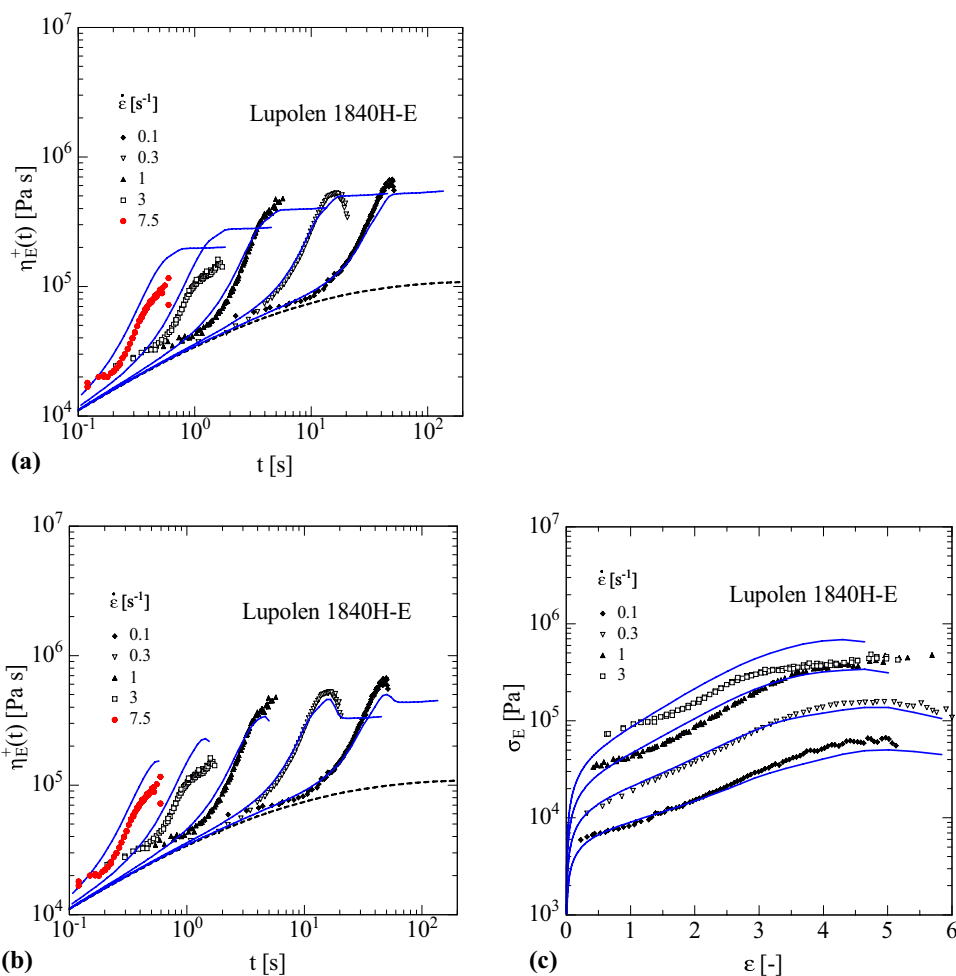
At small deformation rates and/or deformations, the functions H_i reduce to $H_i \rightarrow 1$, and the HMMSF model is recovered. With increasing deformation rate, H_i decreases as soon as $\bar{\lambda}(t, t') > \bar{\lambda}_m$, and the survival probability of entanglements of type i decreases, the more so the larger the strain rate and the larger the value of the weight fraction w_i . For $\bar{\lambda}(t, t') \gg \bar{\lambda}_m$ and elongational flow with constant elongation rate $\dot{\epsilon}$, H_i reduces to

$$H_i = \frac{1}{1 + w_i \tau_i \dot{\epsilon}} \quad (13)$$

At small values of w_i , branch points are only marginally embedded in the temporary polymer network due to large dynamic dilution by chain segments with shorter relaxation times. According to Eq. (13), for small Weissenberg numbers $Wi_i = \tau_i \dot{\epsilon}$, the effect of branch point withdrawal is then relatively small. Only at larger values of Wi_i branch point withdrawal becomes important. Therefore, the quantity relevant for branch point withdrawal is the product of w_i and Wi_i . While the time-dependent elongational stress as determined from Eq. (1) depends on the characteristic stretch parameter $\bar{\lambda}_m$, the steady-state stress depends only on strain rate, LVE characterization, and weight fractions w_i . Thus, the only nonlinear material parameter determining the steady state of elongational stress and viscosity is the dilution modulus G_D according to Eq. (8).

To model fracture of LDPE melts, we adjust the fracture criterion for monodisperse polymers (Wagner et al. 2018, 2021a,b,c) by assuming that fracture occurs as soon as the entanglement

Fig. 4 Comparison of data (symbols) of elongational stress growth coefficient $\eta_E^+(t)$ for LDPE 1840H-E at 150 °C to HMMSF model (lines) with $G_D = 10$ kPa (a), and to EHMMSF model (lines) with $G_D = 10$ kPa and $\bar{\lambda}_m = 90$ (b). Data at $\dot{\epsilon} = 7.5s^{-1}$ were measured at 130 °C and are time-temperature shifted to 150 °C. c Comparison of data (symbols) of elongational stress growth $\sigma_E(\epsilon)$ to EHMMSF model (lines) with $G_D = 10$ kPa and $\bar{\lambda}_m = 90$



segments corresponding to one relaxation mode fracture, i.e., when these segments reach the critical value W_c of the strain energy

$$W_c = 3kTf_{i,c}^2 w_i = U \tag{14}$$

U is the bond-dissociation energy of a single carbon-carbon bond in hydrocarbons. As explained in Wagner et al. (2022), the strain energy of a diluted chain segment is given by $W = 3kTf_i^2 w_i$ with f_i obtained from Eq. (7), and the ratio of bond-dissociation energy U to thermal energy $3kT$ is approximately $U/3kT \approx 35$ and 33 at a temperature of $T = 130$ °C and 150 °C, respectively. According to the entropic fracture hypothesis, when the strain energy of the entanglement segment reaches the critical energy U , the total strain energy of the chain segment will be concentrated on one C-C bond by thermal fluctuations, and this bond then ruptures. This leads to crack initiation and within a few milliseconds to brittle fracture of the sample. Equation (14) defines the square of the critical stretch $f_{i,c}$ at fracture,

$$f_{i,c}^2 = \frac{U}{3kT} \frac{1}{w_i} \tag{15}$$

For the polymers investigated here, fracture is at first triggered by the mode with the longest relaxation time, followed at higher strain rates by fracture of shorter relaxation modes.

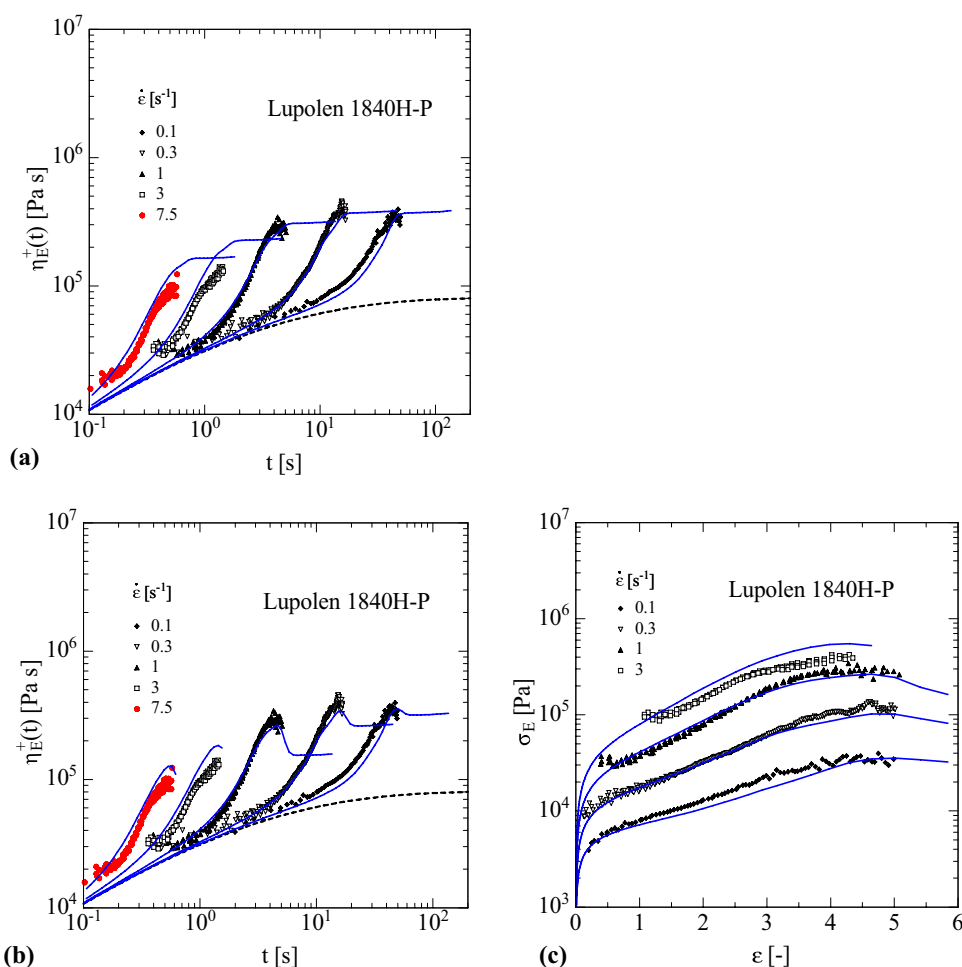
In summary, the parameters of the EHMMSF model including the entropic fracture criterion are LVE, G_D , $\bar{\lambda}_m$, and $U/3kT$, with G_D and $\bar{\lambda}_m$ being the only free model parameters.

Results

Molecular weight, density, and thermal data

The second heating cycle of the DSC results was used to assess the crystallinity of the LDPEs. The percent crystallinity is determined using the following equation (Menczel et al. 2009):

Fig. 5 Comparison of data (symbols) of elongational stress growth coefficient $\eta_E(t)$ for LDPE 1840H-P at 150 °C to HMMSF model (lines) with $G_D = 10$ kPa (a), and to EHMMSF model (lines) with $G_D = 10$ kPa and $\lambda_m = 90$ (b). Data (red symbols) at strain rate $\dot{\epsilon} = 7.5\text{ s}^{-1}$ were measured at 130 °C and are time-temperature shifted to 150 °C. **c** Comparison of data (symbols) of elongational stress growth $\sigma_E(\epsilon)$ to EHMMSF model (lines) with $G_D = 10$ kPa and $\lambda_m = 90$



$$X_c = \frac{\Delta H_m}{\Delta H_m^0} \times 100\% \quad (16)$$

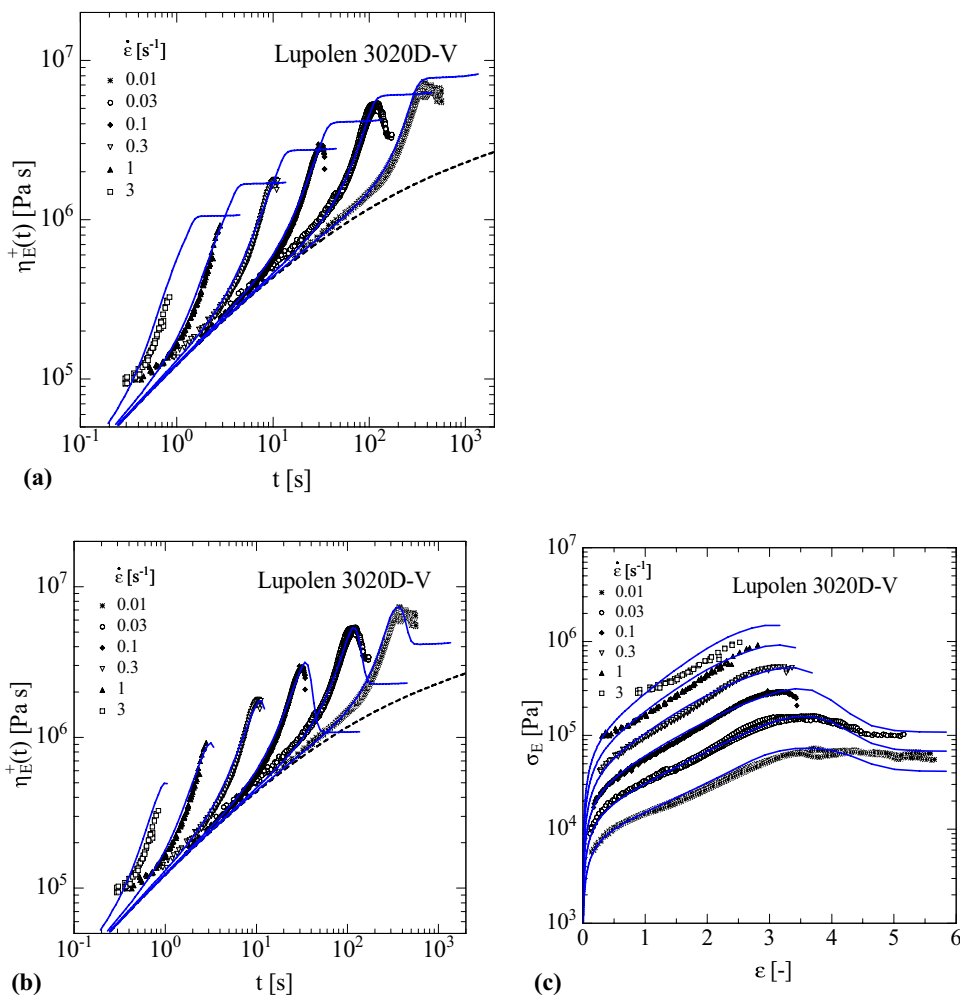
where ΔH_m is the enthalpy of fusion, ΔH_m^0 is the heat of melting of 100% crystalline polymer, and X_c is the percentage crystallinity. The theoretical melting enthalpy of 100% crystalline polyethylene is $\Delta H_m^0 = 293$ J/g (Wunderlich 1973). The density values of the LDPE samples are an average of 5 repetitions. The density results are in agreement with a recent study on these commercial LDPEs where the crystallinity of the samples increases with increasing density (Poh et al. 2022b). The heat flow, molecular weight distribution, and morphology graphs can be found in the Supplementary Information (SI) in Figures S1 to S4. The weight-average molecular weight (Mw), polydispersity index (PDI), degree of branching, density, and crystallinity of the LDPE samples are summarized in Table 2.

Linear-viscoelastic characterization

Figures 1 and 2 show the linear-viscoelastic characterization of the two LDPE melts considered. The mastercurves

of storage (G') and loss modulus (G'') of the virgin sample (V) and the extruded sample (E) of LDPE 1840H (Fig. 1a) do not exhibit much difference; however, the powder sample (P) of LDPE 1840H which was milled to powder at cryogenic temperatures shows definitely lower values of G' and G'' in the terminal regime, and also lower values of the partial relaxation moduli g_i and the relaxation modulus $G(t)$ at larger times (Fig. 1b). This is in agreement with the lower polydispersity of sample LDPE 1840H-P (Table 2) and the lower zero-shear viscosity η_0 (Table 3) compared to samples LDPE 1840H-V and 1840H-E. On the other hand, LDPE 3020D shows significant differences between the mastercurves of G' and G'' and the partial relaxation moduli g_i and the relaxation modulus $G(t)$ at longer times, depending on the three different pre-treatments (Fig. 2): Extrusion of the virgin polymer leads to enhancement of the longest relaxation mode and a significant increase of the zero-shear viscosity η_0 , while cryogenic milling reduces the partial modulus of the longest relaxation time and the zero-shear viscosity η_0 (Table 3). The difference in the behaviors of LDPE 1840H vs. LDPE 3020D regarding extrusion may be explained by the fact that LDPE 1840H is well stabilized,

Fig. 6 Comparison of data (symbols) of elongational stress growth coefficient $\eta_E(t)$ for LDPE 3020D-V at 130 °C to HMMSF model (lines) with $G_D = 3$ kPa (a), and to EHMSF model (lines) with $G_D = 3$ kPa and $\bar{\lambda}_m = 40$ (b). c Comparison of data (symbols) of elongational stress growth $\sigma(\epsilon)$ to EHMSF model (lines) with $G_D = 3$ kPa and $\bar{\lambda}_m = 40$

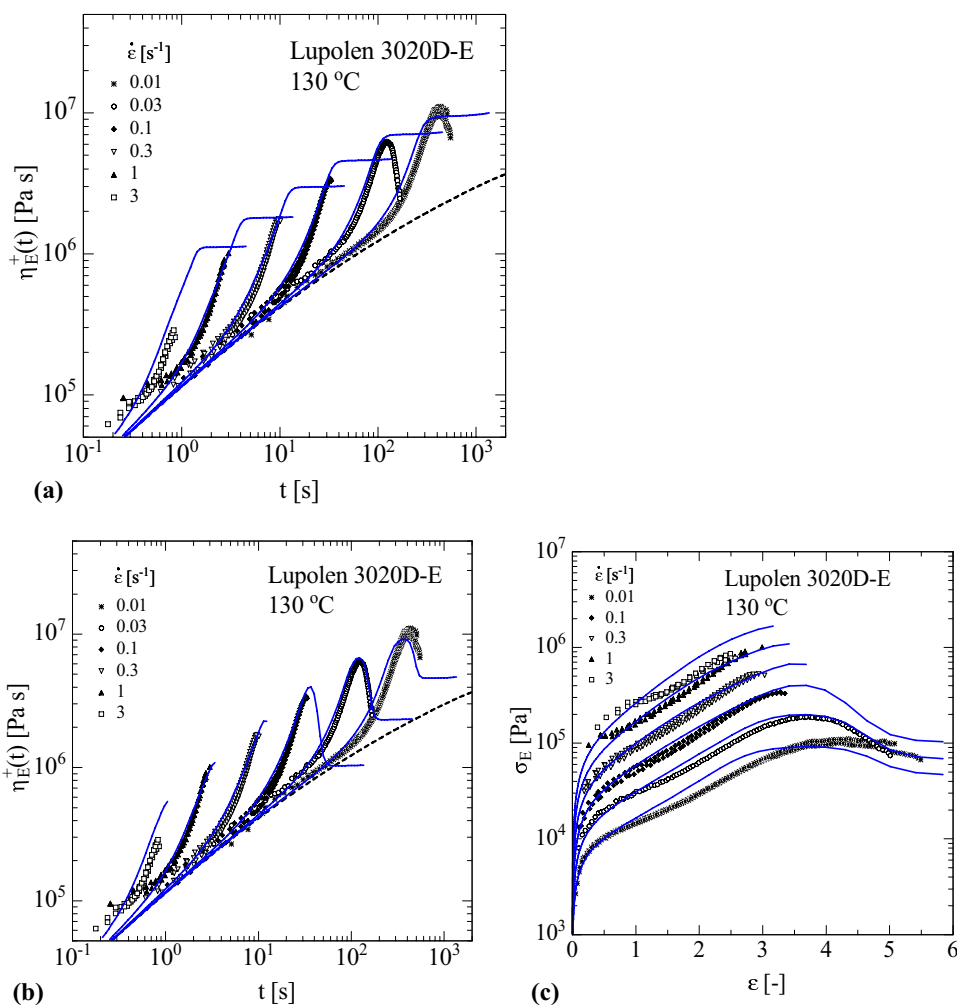


while LDPE 3020D is a polymer which has been stored at ambient conditions for some 20 years resulting in deactivation of the stabilizer. Therefore, during extrusion, LDPE 3020D undergoes oxidation and formation of radicals, which in turn leads to enhanced long-chain branching. On the other hand, the effect of cryogenic milling is clearly seen in both LDPEs. As reported by Liang et al. (2002), strong milling and high-speed collisions lead to the accumulation of mechanical energy in the long chains especially at cryogenic conditions, with the result that covalent bonds rupture. Homolytic cleavage of C-C bonds within the backbone is the cause of mechanochemical polymer degradation. This is in agreement with the significant reduction of the polydispersity index (Table 2) which means that especially the long polymer chains are affected by bond rupture. The relaxation spectra as determined by the IRIS software (Winter and Mours 2006; Poh et al. 2022a) are summarized in the Supplementary Information (Tables S1 and S2).

Elongational stress growth and stress growth coefficient

Figure 3a shows the comparison of the data (symbols) of the elongational stress growth coefficient $\eta_E(t)$ for LDPE 1840H-V at 150 °C to predictions of the HMMSF model (lines) using a dilution modulus of $G_D = 10$ kPa. Data (red symbols) of strain rate $\dot{\epsilon} = 7.5$ s⁻¹ were measured at 130 °C and were time-temperature shifted to 150 °C. Within experimental accuracy, good agreement between data and predictions of the HMMSF model is found up to the maximum value of the stress growth coefficient measured. However, the data indicate a maximum of the stress growth coefficient, while the HMMSF model predicts a steady state. In addition, the samples fracture at $\dot{\epsilon} = 3$ and 7.5 s⁻¹. The maximum can be accounted for by the EHMSF model with $G_D = 10$ kPa and a characteristic stretch parameter $\bar{\lambda}_m = 90$ (Fig. 3b), while the fracture of the samples is found to be in reasonable

Fig. 7 Comparison of data (symbols) of elongational stress growth coefficient $\eta_E(t)$ for LDPE 3020D-E at 130 °C to HMMSF model (lines) with $G_D = 3$ kPa (a), and to EHMSF model (lines) with $G_D = 3$ kPa and $\bar{\lambda}_m = 60$ (b). c Comparison of data (symbols) of elongational stress growth $\sigma(\epsilon)$ to EHMSF model (lines) with $G_D = 3$ kPa and $\bar{\lambda}_m = 60$



agreement with the entropic fracture criterion of Eq. (15). This is even more evident when the elongational stress growth $\sigma(\epsilon)$ is considered (Fig. 3c). According to Wagner et al. (2022), the stretch parameter can be converted in good approximation into an equivalent characteristic Hencky strain by $\epsilon_m \cong 1 + \ln(\bar{\lambda}_m) = 5.5$, with ϵ_m being the Hencky strain of the maximum of the elongational stress in the limit of low strain rates. At higher strain rates, the location of the maximum shifts to lower strains.

As shown in Figs. 4 and 5, with the same parameters set of $G_D = 10$ kPa and $\bar{\lambda}_m = 90$ s (Table 3), the elongational stress growth coefficient $\eta_E(t)$ and the elongational stress growth $\sigma(\epsilon)$ of LDPE 1840H-E and LDPE 1840H-P can be predicted within experimental accuracy. While the HMMSF model gives a good description of the elongational stress growth coefficient $\eta_E(t)$ up to the maximal experimental values (Figs. 4a and 5a), the EHMSF model with the entropic fracture criterion accounts for the maximum of $\eta_E(t)$ and $\sigma(\epsilon)$ seen at lower strain rates, and is in reasonable agreement with the fracture of the filaments found at higher strain rates. At the elongation rates of 1

s^{-1} and $3 s^{-1}$, the fracture criterion according to Eq. (15) is reached by the longest relaxation time, at $7.5 s^{-1}$ by the second longest relaxation time.

Figures 6, 7, 8, and 9 show the data (symbols) of the elongational stress growth coefficient $\eta_E(t)$ and the elongational stress growth $\sigma(\epsilon)$ of LDPE 3020D measured at 130 °C. The sample LDPE 3020D-E was also measured at 150 °C, and the data (red symbols) were time-temperature shifted to 130 °C, resulting in excellent agreement (Fig. 8). In the case of LDPE 3020D, the type of sample pre-treatment has not only an effect on the linear-viscoelastic properties as discussed in the “Linear-viscoelastic characterization” chapter, but also affects the characteristic stretch parameter $\bar{\lambda}_m$ (Table 3). Within experimental accuracy, good agreement between data and predictions of the HMMSF model using a dilution modulus of $G_D = 3$ kPa is found up to the maximal values of the elongational stress growth coefficient $\eta_E(t)$ measured, independent of the pre-treatment methods (Figs. 6a, 7a, and 9a). However, while the maxima of $\eta_E(t)$ (Figs. 6b and 9b) and $\sigma(\epsilon)$ (Figs. 6c and 9c) found at lower strain rates are in agreement with the EHMSF model using a characteristic stretch parameter of $\bar{\lambda}_m = 40$, the

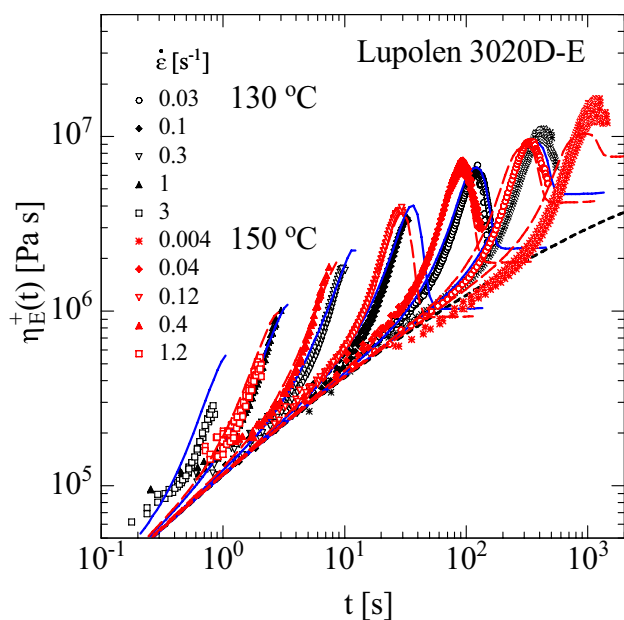
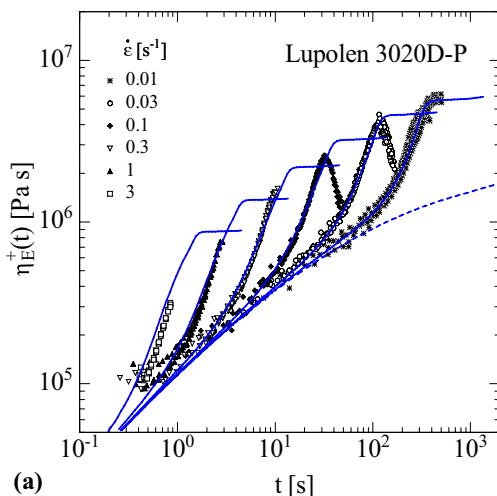
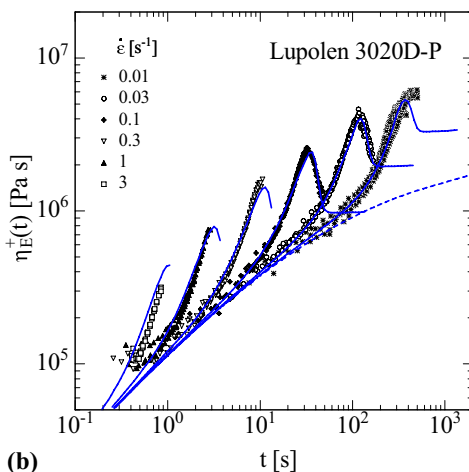


Fig. 8 Comparison of data (symbols) of elongational stress growth coefficient $\eta_E(t)$ for LDPE 3020D-E at 130 °C to EHMMSF model (lines) with $G_D = 3$ kPa and $\bar{\lambda}_m = 60$. Data (red symbols) measured at 150 °C are time-temperature shifted to 130 °C

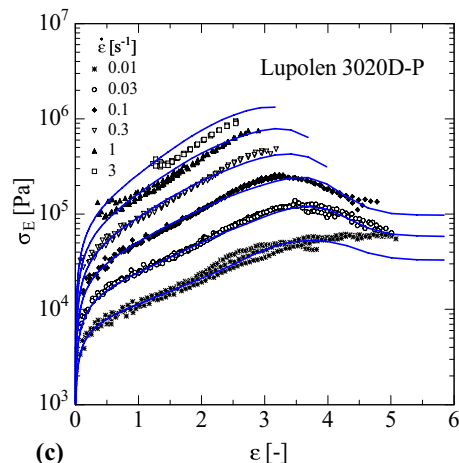
Fig. 9 Comparison of data (symbols) of elongational stress growth coefficient $\eta_E(t)$ for LDPE 3020D-P at 130 °C to HMMSF model (lines) with $G_D = 3$ kPa (a), and to EHMMSF model (lines) with $G_D = 3$ kPa and $\bar{\lambda}_m = 40$ (b). **c** Comparison of data (symbols) of elongational stress growth $\sigma(\epsilon)$ to EHMMSF model (lines) with $G_D = 3$ kPa and $\bar{\lambda}_m = 40$



(a)



(b)



(c)

extruded sample LDPE 3020D-E (Figs. 7b and c, Fig. 8) shows maxima of $\eta_E(t)$ and $\sigma(\epsilon)$ at higher strains corresponding to a characteristic stretch parameter of $\bar{\lambda}_m = 60$. As discussed above, LDPE 3020D-E undergoes oxidation and formation of radicals during extrusion leading to enhanced long-chain branching. Irrespective of sample preparation, the entropic fracture criterion of Eq. (15) implemented in the stress Eq. (1) of the EHMMSF model is again found to be in general agreement with the fracture of the samples observed at higher strain rates, and greatly improves the overall predictions of the EHMMSF model. At the elongation rates of 0.3 s^{-1} and 1 s^{-1} , the fracture criterion according to Eq. (15) is reached by the longest relaxation time, at 3 s^{-1} by the second longest relaxation time.

High-speed videography of fracture

Figures 10 and 11 show the optical observation of fracture development in LDPE 1840H and 3020D captured at an elongation rate of 3.0 s^{-1} and a temperature of 130 °C in sequence from left to right using high-speed videography at 16,000

and 25,000 frames per second, respectively. The high-speed videography of fracture of the LDPE samples was repeated three times for each LDPE and sample preparation method, and the frames can be found in the Supplementary Information (Figures S5 to S10). As typical examples, fracture events of LDPE 1840H samples (Fig. 10) and LDPE 3020D samples (Fig. 11) are shown here. The filaments of 1840H can be stretched longer and to thinner filaments before fracture occurs as compared to samples of 3020D. This is in agreement with the elongational stress growth data of Figs. 3, 4, 5, 6, 7, 8, and 9 which show that fracture of 1840H occurs typically at Hencky strains ϵ between 4 and 5, while fracture of filaments of 3020D is observed at lower Hencky strains of 2.5 to 3.5. Due to the thin filament observed in the sequence of images captured for the 1840H samples (Fig. 10), it is difficult to follow the initiation and propagation of the crack in detail, and to observe the fracture tip profile. In contrast, the

samples of 3020D fracturing at much lower stretch show the appearance of a parabolic crack opening (Fig. 11) that has all the signatures of an elastic fracture following the viscoelastic trumpet model of de Gennes (1996). Crack openings start always at the sample surface. Similar parabolic crack openings have been observed earlier by Huang et al. (2016), and Huang and Hassager (2017) for monodisperse polystyrene solutions. They showed that polymeric systems have just two states, liquid or solid, and that a clear distinction exists between the liquid state (infinite steady-state elongation) and the solid state (fracture).

Within the unavoidable experimental scatter expected for fracture events, we could not identify significant differences in the fracture of samples with different pre-treatments, which means that even sample “V” compression molded from pellets as received is sufficiently homogeneous and do not fail at grain boundaries as originally suspected.

Fig. 10 Sequence of images captured at 16,000 fps of the propagation of fracture in uniaxial extensional flow of **a** 1840H-V1 and **b** 1840H-E3 stretched at 3.0 s^{-1} at $130 \text{ }^\circ\text{C}$ from left to right. The time $t = 0$ is set at the frame where the filament breaks and the times of the frames indicate the time before fracture

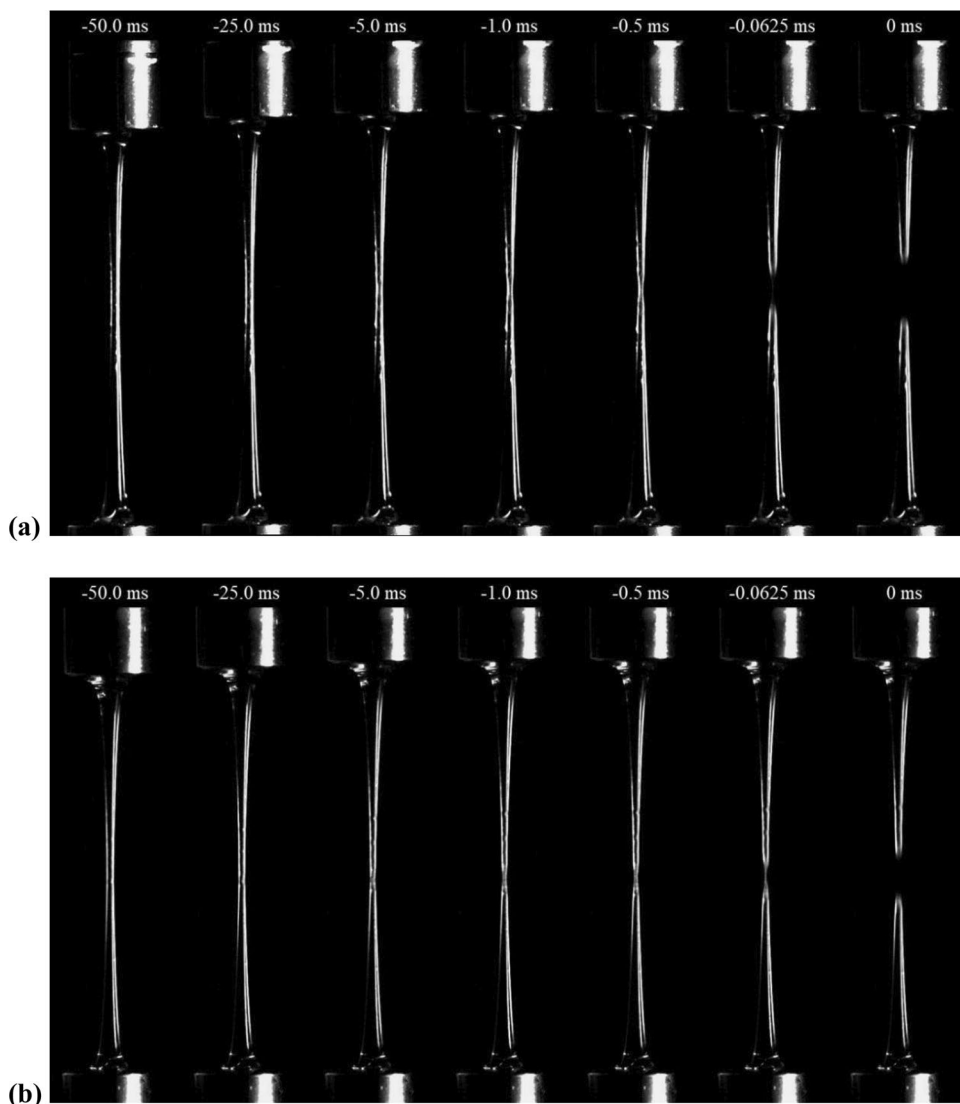
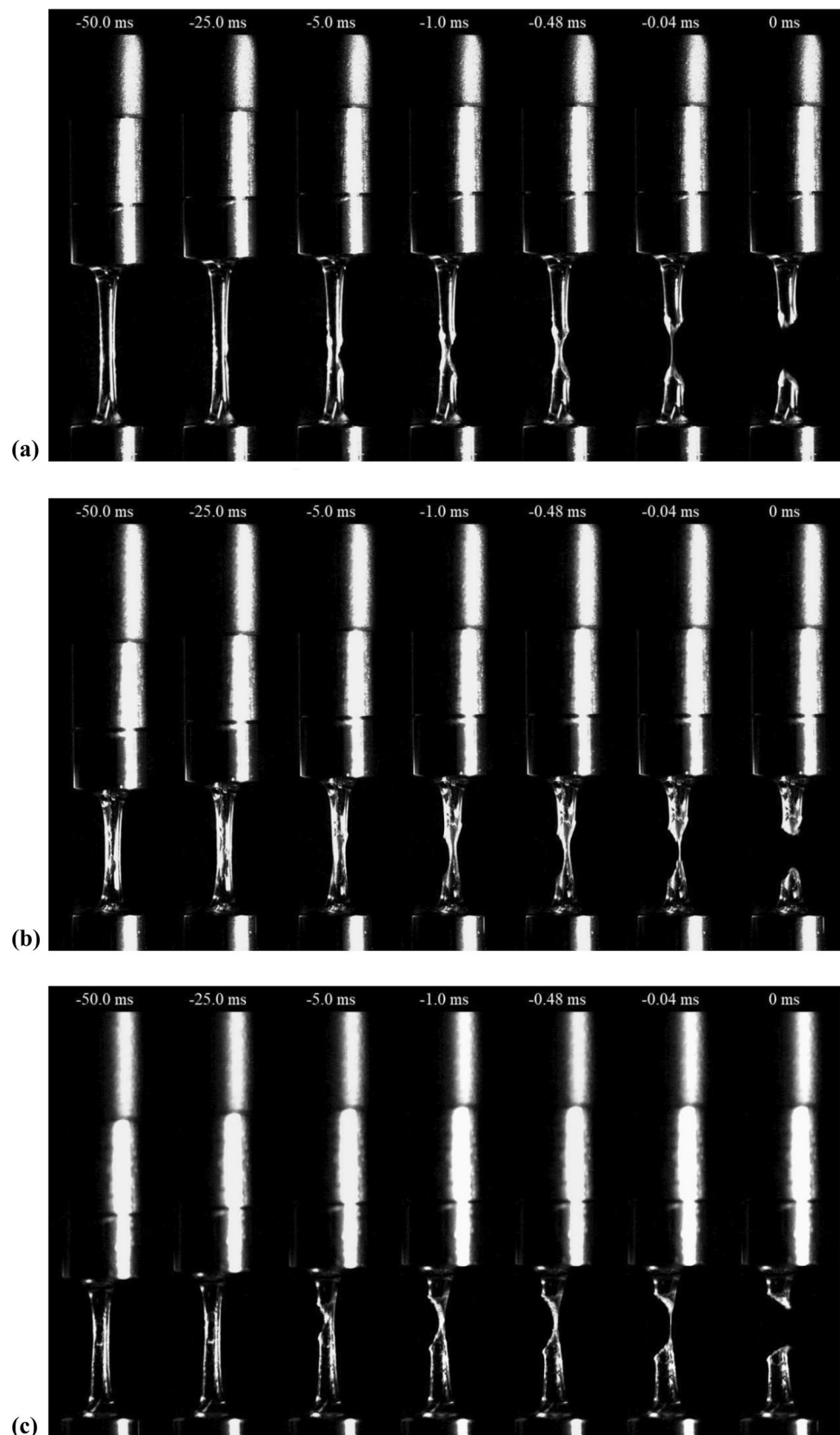


Fig. 11 Sequence of images shot at 25,000 fps of the propagation of fracture in uniaxial extensional flow of **a** 3020D-V1, **b** 3020D-E2, and **c** 3020D-P2 stretched at 3.0 s^{-1} at $130 \text{ }^\circ\text{C}$ from left to right. The time $t = 0$ is set at the frame where the filament breaks and the times of the frames indicate the time before fracture



Discussion and conclusions

The Hierarchical Multi-mode Molecular Stress Function (HMMSF) model (Wagner et al. 2022) is based on the fact that the rheological effect of polydispersity and, in the case of LCB polymers, the effect of the often unknown molecular branching topology is already contained in the linear-viscoelastic spectrum of relaxation times of the polymer. Therefore, only a very limited number of well-defined constitutive assumptions concerning the nonlinear rheology is needed, thereby reducing the number of adjustable free nonlinear material parameters to a minimum. The HMMSF model, with only one nonlinear material parameter, the dilution modulus G_D , has been shown to quantitatively model the extensional viscosities of linear polymer melts at all deformation rates investigated (Narimissa and Wagner 2016c). For long-chain branched polymer melts, the HMMSF model describes accurately the elongational stress growth coefficient up to the maximum of the elongational viscosity, but fails to predict the maximum and the following steady-state viscosity at higher strain rates. For the two LDPEs investigated here, the values of the dilution modulus G_D are 3 kPa (LDPE 3020D) and 10 kPa (LDPE 1840H), independent of the pre-treatment method applied. This shows clearly that the effect of the different pre-treatment methods of the samples affects primarily the LVE behavior.

To account for the maximum in the transient elongational viscosity, the EHMSF model takes into account branch point withdrawal in the elongational flow of LCB melts and allows quantifying the maximum in the transient elongational viscosity of LDPE melts observed at higher strain rates and higher strains by a single characteristic stretch parameter $\bar{\lambda}_m$. For LDPE 1840H, the stretch parameter was found to be $\bar{\lambda}_m = 90$, independent of the pre-treatment of the samples. In contrast, while the stretch parameter for LDPE 3020D-V and LDPE 3020D-P is $\bar{\lambda}_m = 40$, a value of $\bar{\lambda}_m = 60$ was found for LDPE 3020D-E. According to Eq. (11), at constant $\bar{\lambda}_m$ the maximum will be reached at smaller Hencky strains with increasing strain rate and will be more pronounced, in agreement with experimental evidence. A larger value of $\bar{\lambda}_m$ as in the case of LDPE 3020D-E compared to LDPE 3020D-V and LDPE 3020D-P is associated with a polymer topology featuring a larger number and/or longer side chains resulting in a larger deformation and thereby a larger tensile force in the backbone chain required for branch point withdrawal. This is in agreement with the expectation that LDPE 3020D-E undergoes oxidation and radical formation during extrusion causing a buildup of long-chain branching.

Hence, starting from the linear-viscoelastic relaxation modulus $G(t)$, it is possible to characterize the nonlinear-viscoelastic elongational flow properties of LDPE melts by only two material parameters, the dilution modulus G_D and the stretch parameter $\bar{\lambda}_m$. This can be of considerable importance for both polymer characterization as well as polymer processing simulations.

The entropic fracture criterion was found to be of decisive importance for the predictive capabilities of the EHMSF at higher strain rates. According to this criterion, a polymer will fail by fracture when the stretch energy of one relaxation mode reaches the bond-dissociation energy of a single carbon-carbon bond. For both LDPE 1840H and LDPE 3020D, and for all pre-treatment methods, fracture was observed at the higher strain rates investigated and in reasonable agreement with the entropic fracture criterion. High-speed videography reveals that fracture is preceded by a parabolic crack opening characteristic for elastic fracture according to the viscoelastic trumpet model of de Gennes (1996), which has been observed earlier (Huang et al. 2016; Huang and Hassager 2017) in the case of monodisperse polystyrene solutions. Here, for the first time to our knowledge, we demonstrate the appearance of a parabolic crack opening initiating the fracture process of polydisperse and long-chain branched LDPE.

Supplementary Information The online version contains supplementary material available at <https://doi.org/10.1007/s00397-023-01392-1>.

Funding Open Access funding enabled and organized by Projekt DEAL. This work was supported by the Shantou Science and Technology Bureau (200909094890694).

Open Access This article is licensed under a Creative Commons Attribution 4.0 International License, which permits use, sharing, adaptation, distribution and reproduction in any medium or format, as long as you give appropriate credit to the original author(s) and the source, provide a link to the Creative Commons licence, and indicate if changes were made. The images or other third party material in this article are included in the article's Creative Commons licence, unless indicated otherwise in a credit line to the material. If material is not included in the article's Creative Commons licence and your intended use is not permitted by statutory regulation or exceeds the permitted use, you will need to obtain permission directly from the copyright holder. To view a copy of this licence, visit <http://creativecommons.org/licenses/by/4.0/>.

References

- de Gennes PG (1996) Soft Adhesives. *Langmuir* 12:4497–4500
- Doi M, Edwards SF (1978) Dynamics of concentrated polymer systems. Part 3—the constitutive equation. *J Chem Soc Faraday Trans 2: Mol Chem Phys* 74:1818–1832
- Huang Q et al (2016) Multiple cracks propagate simultaneously in polymer liquids in tension. *Phys Rev Lett* 117:087801
- Huang Q, Hassager O (2017) Polymer liquids fracture like solids. *Soft Mat* 13:3470–3474

- Liang SB et al (2002) Production of fine polymer powder under cryogenic conditions. *Chem Eng Technol* 25:401–405
- McLeish TCB, Larson RG (1998) Molecular constitutive equations for a class of branched polymers: the pom-pom polymer. *J Rheol* 42:81–110
- Menczel JD et al. (2009) Differential scanning calorimetry (DSC), in *Thermal Analysis of Polymers*, p. 7–239. <https://doi.org/10.1002/9780470423837.ch2>.
- Narimissa E, Wagner MH (2016a) A hierarchical multi-mode MSF model for long-chain branched polymer melts part III: shear flow. *Rheol Acta* 55:633–639
- Narimissa E, Wagner MH (2016b) From linear viscoelasticity to elongational flow of polydisperse polymer melts: the hierarchical multi-mode molecular stress function model. *Polymer* 104:204–214
- Narimissa E, Wagner MH (2016c) A hierarchical multi-mode molecular stress function model for linear polymer melts in extensional flows. *J Rheol* 60:625–636
- Narimissa E, Wagner MH (2019a) Review of the hierarchical multi-mode molecular stress function model for broadly distributed linear and LCB polymer melts. *Poly Eng Sci* 59:573–583
- Narimissa E, Wagner MH (2019b) Review on tube model based constitutive equations for polydisperse linear and long-chain branched polymer melts. *J Rheology* 63:361–375
- Narimissa E, Rolón-Garrido VH, Wagner MH (2015) A hierarchical multi-mode MSF model for long-chain branched polymer melts part I: elongational flow. *Rheol Acta* 54:779–791
- Narimissa E, Rolón-Garrido VH, Wagner MH (2016) A hierarchical multi-mode MSF model for long-chain branched polymer melts part II: multiaxial extensional flows. *Rheol Acta* 55:327–333
- Poh L et al (2022a) Interactive shear and extensional rheology—25 years of IRIS software. *Rheol Acta* 61:259–269
- Poh L et al (2022b) Characterization of industrial low-density polyethylene: a thermal, dynamic mechanical, and rheological investigation. *Rheol. Acta* 61:701–720
- Román Marín JM et al (2013) A control scheme for filament stretching rheometers with application to polymer melts. *J Non-Newtonian Fluid Mech* 194:14–22
- Wagner MH (2011) The effect of dynamic tube dilation on chain stretch in nonlinear polymer melt rheology. *J Non-Newtonian Fluid Mech* 166:915–924
- Wagner MH, Rolón-Garrido VH (2009a) Nonlinear rheology of linear polymer melts: modeling chain stretch by interchain tube pressure and Rouse time. *Korea-Australia Rheolol J* 21:203–211
- Wagner MH, Rolón-Garrido VH (2009b) Recent advances in constitutive modeling of polymer melts. *Novel Trends of Rheology III*. AIP Conf Proc 1152:16–31. <https://doi.org/10.1063/1.3203266>
- Wagner MH, Kheirandish S, Hassager O (2005) Quantitative prediction of transient and steady-state elongational viscosity of nearly monodisperse polystyrene melts. *J Rheology* 49:1317–1327
- Wagner MH, Narimissa E, Huang Q (2018) On the origin of brittle fracture of entangled polymer solutions and melts. *J Rheol* 62:221–223
- Wagner MH, Narimissa E, Huang Q (2021a) Scaling relations for brittle fracture of entangled polystyrene melts and solutions in elongational flow. *J Rheol* 65:311–324
- Wagner MH, Narimissa E, Poh L, Shahid T (2021b) Modelling elongational viscosity and brittle fracture of polystyrene solutions. *Rheol Acta* 60:385–396
- Wagner MH, Narimissa E, Shahid T (2021c) Elongational viscosity and brittle fracture of bidisperse blends of a high and several low molar mass polystyrenes. *Rheol Acta* 60:803–817
- Wagner MH, Narimissa E, Poh L, Huang Q (2022) Modelling elongational viscosity overshoot and brittle fracture of low-density polyethylene melts. *Rheol Acta* 61:281–298
- Winter HH, Mours M (2006) The cyber infrastructure initiative for rheology. *Rheol Acta* 45:331–338
- Wunderlich B (1973) *Macromolecular physics*. Academic Press, New York (N.Y.)

Publisher's note Springer Nature remains neutral with regard to jurisdictional claims in published maps and institutional affiliations.